Applied Catalysis B: Environmental 182 (2016) 33–46

Contents lists available at ScienceDirect

Applied Catalysis B: Environmental

journal homepage: www.elsevier.com/locate/apcatb

Steam reforming of *n*-butanol over Rh/ZrO_2 catalyst: role of 1-butene and butyraldehyde

Heikki Harju[a], Juha Lehtonen[a], Leon Lefferts[a,b,*]

[a] *Research Group of Industrial Chemistry, Department of Biotechnology and Chemical Technology, School of Chemical Technology, Aalto University, PO Box 16100, 00076 Aalto, Finland*

[b] *Catalytic Processes and Materials, Department of Science and Technology, MESA+ Institute for Nanotechnology, University of Twente, PO Box 217, 7500 AE Enschede, The Netherlands*

ARTICLE INFO

Article history:
Received 18 June 2015
Received in revised form 31 August 2015
Accepted 2 September 2015
Available online 8 September 2015

Keywords:
Butanol steam reforming
Rhodium
Reaction pathway
Catalyst deactivation
Temperature programmed oxidation

ABSTRACT

Steam reforming (SR) of *n*-butanol and its main reaction intermediates, i.e., 1-butene, and butyraldehyde, was studied over 0,5 wt.% Rh/ZrO_2 catalyst at 500 and 700 °C, atmospheric pressure and steam to carbon (S/C) molar ratio of 4. Coke deposits on the spent catalyst samples were characterized using temperature programmed oxidation (TPO) and CHNS + O elemental analysis. Catalyst performance, i.e., conversion, product distribution and short term stability, as well as coke deposit characterization, were utilized to develop reaction networks for 1-butene, butyraldehyde and butanol. At 500 °C the individual reforming rates of the three components decrease in the order butyraldehyde > butanol > 1-butene and the initial reaction rates of butanol decrease in the order dehydration > dehydrogenation > direct reforming. The three main pathways, i.e., direct reforming of butanol and reforming via butane and butyraldehyde respectively, contributed roughly equally to the butanol reforming activity of the catalyst at 500 °C. At 700 °C, complete conversion was observed for all components, with hydrogen yields 70% of theoretical maximum for butanol and 1-butene and 60% for butyraldehyde. Deactivation of the catalyst for reforming is caused by carbon deposition on and near the Rh particles. The deposition is a side reaction of the reforming surface reaction and decreases in the order of magnitude butyraldehyde > butanol » 1-butene. Carbon deposition elsewhere on the support proceeds mainly via the coupling products of butyraldehyde.

1. Introduction

Hydrogen is a key element in conventional and emerging energy systems. It is essential in many refinery operations, including hydro-deoxygenation (HDO) of bio-based feedstock and the recent announcements in starting mass production of fuel cell powered cars predict an increasing consumption of hydrogen directly as an automotive fuel. Renewable alternatives are required for the conventional unsustainable method of producing hydrogen through steam reforming (SR) of natural gas. Bio-hydrogen, i.e., hydrogen from biomass, can be produced through several methods [1], including direct gasification and catalytic reforming of bio based intermediates, e.g., flash pyrolysis oil [2,3], ethanol [4–8] or butanol from ABE fermentation [9–14]. Flash pyrolysis oil, and the aqueous fraction thereof, is a complex mixture containing e.g. acetic acid [15–19], phenol [20–24] and enough butanol [25] to make it an interesting model compound for two different bio-based feedstocks.

Steam reforming (SR) of light alcohols has been widely studied and reviews are available [4,26], but the literature on reforming of butanol is much less abundant. A few groups have studied SR of butanol using Ni/Al_2O_3 based [27–31], Co based [10] and Rh based catalyst systems [7,8,32]. Autothermal reforming (ATR) of butanol has also attracted some attention, both as a pure compound over Rh and Ni catalysts [32,33] and as a part of the ABE-fermentation product mix over Co based catalysts [11–14].

Conventional Ni based reforming catalysts may not be the best choice for reforming of alcohols, as Ni is well known to be prone to formation of whisker carbon in the presence of olefins [34] readily formed through the dehydration reaction of alcohols on oxide supports. On the other hand, zirconia and zirconia mixed oxide supported catalysts have shown promising results for the reforming of ethanol with Rh [6] and other metals [5,35] and other oxygenates with Rh [20–24,36] and other metals [15,16,18,19]. In our

* Corresponding author at: Catalytic Processes and Materials, Department of Science and Technology, MESA+ Institute for Nanotechnology, University of Twente, PO Box 217, 7500 AE Enschede, Netherlands. Fax: +31 53 489 4683.
E-mail addresses: heikki.harju@aalto.fi (H. Harju), juha.lehtonen@aalto.fi (J. Lehtonen), l.lefferts@utwente.nl (L. Lefferts).

http://dx.doi.org/10.1016/j.apcatb.2015.09.009
0926-3373/

previous work [32], it was shown that Rh supported on ZrO_2 was active, selective and stable at 700 °C, even with low metal loading of 0,5 wt.%. However, at lower temperatures the catalyst deactivated rapidly due to coke deposition on or near the Rh particles. It was observed that the reforming of butanol proceeds through several parallel pathways, namely by direct reforming and through 1-butene and butyraldehyde intermediates. The results also indicated that coke deposition was more likely linked to butyraldehyde rather than 1-butene, as is often asserted. In this work the reaction scheme is further developed for butanol steam reforming and the most important processes leading to coke deposition are identified based on reforming experiments of both main reaction intermediates, i.e., 1-butene and butyraldehyde.

Experimental

2.1. Catalyst preparation and characterization

The Rh catalyst was prepared by vacuum assisted dry impregnation from 10 wt.% $Rh(NO_3)_3$ solution diluted in 5 wt.% nitric acid (Sigma–Aldrich) to obtain 0.5% Rh by weight. The ZrO_2 support (MEL Chemicals EC0100) was ground and screened to particle size 0.25–0.42 mm and calcined in synthetic air (20% O_2/N_2, Aga, 99.99%) at 850 °C for 16 h. Prior to impregnation, the support was dried overnight at 90 °C and one hour under vacuum at 100 °C. The catalyst was kept under vacuum during the impregnation and subsequent drying, first at room temperature overnight, then at 40 °C for 1.5 h and 60 °C for 0.5 h, before being calcined at 850 °C for 1 h (heating rate 80 °C/h). The Al_2O_3 (Akzo 001/1.5E) was ground, screened and calcined according to the same procedure as the ZrO_2.

The Rh loading of the fresh catalyst was determined by X-ray fluorescence spectrometer (Philips PW 1480 XRF) equipped with UniQuant 4-software. The BET surface area of the ZrO_2 and Al_2O_3 were measured using 11 point BET method in Quantachrome Autosorb 1 and H_2 chemisorption was performed with Coulter Omnisorp 100 CX, using methods described elsewhere [37,38].

2.2. Reaction experiments

Tubular quartz reactor with inner diameter 7 mm was packed with 0.1 g of the catalyst sandwiched between two 0.3 g layers of SiC grains and placed in a three-zone furnace equipped with a temperature controller (Carbolite). The catalyst bed temperature was measured with a thermocouple inserted in a quartz pocket (outer diameter 3.1 mm) running through the catalyst bed. To limit the empty space in the reactor, the inner diameter of the reactor tube was reduced to 4 mm after the catalyst bed and the outer diameter of the thermocouple pocket was widened to 6 mm above the catalyst bed. With the thermocouple in place, the height of the catalyst layer was 2 mm.

The reactor was heated to 600 °C under Ar (Aga, 99.999%) flow, followed by reduction in 50% H_2 (Aga, 99.999%) in Ar for one hour, after which the reactor was flushed with Ar and heated or cooled to the desired reaction temperature in Ar atmosphere. The reduction temperature was chosen based on literature [39] to ensure complete reduction of Rh.

The tested feeds were *n*-butanol (Sigma–Aldrich, 99.4%), butyraldehyde (Fluka, 99.0%), 1-butene (Aga, 99.5%) and 9:1 mixtures of butanol and either butyraldehyde or butene. 0.05 ml/min liquid hydrocarbon and 0.16.ml/min distilled water were fed into separate evaporators (180 °C) by high performance liquid chromatography pumps (HPLC-pumps, Agilent Technologies), equipped with micro vacuum degassers (Agilent Technologies). 1-butene (11 ml/min, NTP) and/or Ar (180 ml/min, NTP) were introduced using gas mass flow controllers (Brooks) and mixed with the vaporized components before introduction to the reactor. The total flow rate of the reaction mixture in the inlet temperature of the reactor (180 °C) was 650 ml/min, translating to GHSV 101,000 h^{-1} and implying a contact time of typically 20 ms. The composition of the reaction mixture by volume was 3% hydrocarbon, 50% H_2O and 47% Ar. The temperature of the catalyst bed was kept constant during the experimental runs (typically 150 min) by adjusting the set-point temperature of the furnace.

External diffusion limitation can be excluded based on calculation of Mears' criterion C_M [40], resulting in $C_M \approx 7.8{*}10^{-5} \ll 0.15$. Occurrence of any internal diffusion limitation for steam reforming at 500 °C was estimated with the Weisz-Prater criterion C_{WP} [41], based on the apparent kinetics, resulting in $C_{WP} \approx 40$, indicating that the influence of internal diffusion on the reaction rates is significant. Naturally, any influence of internal diffusion will become more dominant when increasing the temperature to 700 °C.

For comparative purposes, and in order to see which products originate from surface reactions on the support or from gas phase reactions, experiments were also carried out with pure ZrO_2 and blank experiments were done using a bed of 0.6 g SiC filler. Butyraldehyde and 1-butene were also tested over bare Al_2O_3 in order to test how increased support acidity would affect coke deposition on the bare support. To probe the regenerability of the catalyst, up to three repeat experiments were carried out with the same sample of catalyst, regenerating the catalyst by TPO between the runs.

2.3. Product analysis and calculation

The product gas mixture leaving the reactor was diluted with N_2 (1600 ml/min, NTP) and analyzed using an online Fourier transform infrared (FTIR) spectrometer (Gasmet™) equipped with a Peltier-cooled mercury-cadmium-telluride (MCT) detector and quantitative multicomponent analysis software (Calcmet). The sample cell was kept at 180 °C to prevent any condensation. The compounds analyzed were H_2O, CO, CO_2, CH_4, acetylene, ethylene, ethane, and propylene, all isomers of butene, butanol, butyraldehyde and butyric acid. It was not possible to analyze *n*-butane and propane together with the C_4 oxygenates because of excessive interference in the analysis. Downstream of the FTIR analysis, water and any other condensable compounds were removed in a Peltier-cooled PSS-10 gas drier (M&C) and the dry gas was further analyzed with a set of GMS810 gas analyzers (SICK), with modules for H_2, CO_2, CO and CH_4. Further downstream, the flow rate of the dry gas was measured using a volumetric gas meter. After the experiment, a sample was taken from the organic phase of the condensate, which contains also an aqueous phase, collected by the gas drier and analyzed with GC/MS for a qualitative analysis of the condensable compounds produced.

The hydrogen yield was calculated based on the theoretical stoichiometric maximum of butanol conversion to H_2 and CO_2 (H_2/butanol = 12 mol/mol).

$$Y_{H_2} = \frac{F_{H_{2out}}}{12F_{Bu} \times OH_{in}} \quad (1)$$

The yields of components other than H_2 were defined on C_1 basis. Yield of compound *i* is therefore the ratio of the moles of carbon in compound *i* (molar flow of compound *i* in the product in moles/min, $F_{i,out}$, multiplied by the carbon number of the compound, N_{Ci}) to the total molar amount of carbon in the feed (mol C_i/mol C_{in}):

$$Y_i \frac{F_{iout} N_{c_i}}{F_{Bu} OH_{in} \times 4} \quad (2)$$

Products that could not be detected by the online FTIR or the GMS810 analyzers were lumped as unidentified products. The yield of unidentified products was calculated from the mass balance as

the difference between identified products and total amount of carbon.

2.4. Characterization of spent catalyst

After the experiment, the reactor was flushed with Ar and cooled down to room temperature. The amount of carbon on the used catalysts was determined by temperature programmed oxidation (TPO) in the same setup without opening the reactor in between. The catalyst was heated at 5 °C/min to 800 °C in 3% O_2 in Ar and N_2 (650 ml/min), kept at 800 °C for 1 h to ensure total removal of deposits and then allowed to cool down. Products were analyzed with the FTIR and GMS810 analyzers described above. The only observed product during TPO was CO_2, except for Al_2O_3 spent in butyraldehyde reforming, for which also CO was observed.

In order to study the elemental composition of the carbon deposits, coked catalyst samples were obtained by removing the catalyst from the reactor after the reaction experiment and sieving it in order to separate the SiC filler from the sample. The N, C, H, S and O content of the coked samples were determined using FLASH 2000 series analyzer. The samples, typically 2 mg, were weighted in tin/silver capsules, placed inside the Thermo Scientific MAS 200R auto-sampler at a pre-set time, and then dropped into an oxidation/reduction reactor kept at a temperature of 900–1000 °C. The exact amount of oxygen required for optimum combustion of the sample was delivered into the combustion reactor at a precise time. The reaction of oxygen with the tin capsule at elevated temperature generates an exothermic reaction which raises the temperature to 1800 °C for a few seconds. At this high temperature, both organic and many inorganic substances are converted into elemental gases which, after further reduction, were separated in a chromatographic column and finally detected by a highly sensitive thermal conductivity detector (TCD). The determination of oxygen was done via pyrolysis in He flow (Aga, 99,999 %) at a temperature of 1060 °C in the same analyzer. Results were calculated using Certified Elemental Microanalysis standards (CHNS/CHNS-O Standards Kit: Cystine, Sulphanilamide, Methionine and BBOT: Catalogue Code.Thermo: 33,840,010). Each coked sample was analyzed three times for both O and N, C, H and S contents.

3. Results

3.1. Catalyst characterization

The BET surface area of the ZrO_2 support was 45 m^2/g and the Al_2O_3 was 250 m^2/g. The metal loading measured by XRF was 0.57 ± 0.03 wt.%, similar to the targeted loading of 0.5%. Rh dispersion was 22% according to H_2 chemisorption.

3.2. Conversions

3.2.1. Conversions at 500 °C

Fig. 1 shows the change of conversion of butanol over time at 500 °C in both pure and mixed feeds, for Rh/ZrO_2 as well as bare ZrO_2 and in the absence of catalyst. Initially, the conversion of butanol mixed with 1-butene declines more gradually than the conversion of pure butanol, while the conversion of butanol mixed with butyraldehyde declines more rapidly. However, after ca. 30 min the decline rate of conversion of pure butanol becomes slower than in the mixed feeds. The final conversion of butanol in both mixed feeds is lower than in the pure feed. The conversions of butanol in all feeds approach the conversions observed on bare ZrO_2 in Fig. 1B, indicating deactivation of the Rh sites. The lower conversion of butanol in the mixed feeds over bare ZrO_2 indicates competition between butanol and the intermediates on the support surface.

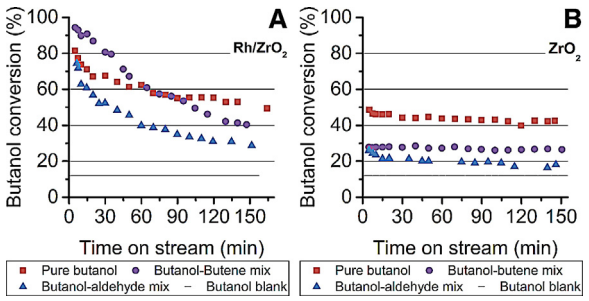

Fig. 1. Conversion of butanol at 500 °C, S/C ratio 4. (A) Rh/ZrO_2 (B) ZrO_2.

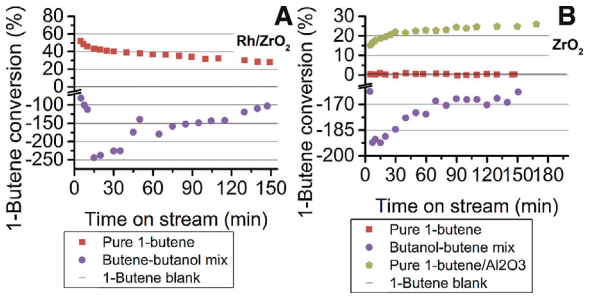

Fig. 2. Conversion of 1-butene at 500 °C, S/C ratio 4. (A) Rh/ZrO_2 (B) ZrO_2 and Al_2O_3.

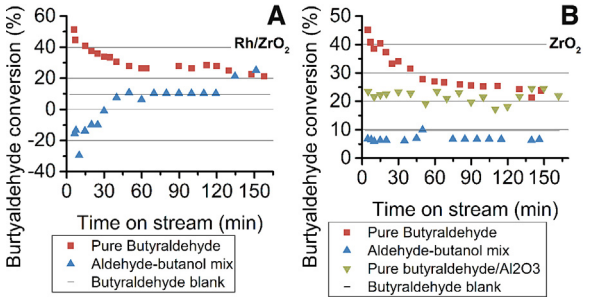

Fig. 3. Conversion of butyraldehyde at 500 °C, S/C ratio 4. (A) Rh/ZrO_2 (B) ZrO_2 and Al_2O_3.

Fig. 2 shows the conversion of 1-butene at 500 °C in both pure and mixed feeds, for Rh/ZrO_2 as well as bare ZrO_2, bare Al_2O_3 and in the absence of catalyst. Conversion of pure 1-butene is considerably lower than butanol on Rh/ZrO_2, both initially and after 150 min. The negative conversion of 1-butene observed for the mixed feed over both Rh/ZrO_2 and bare ZrO_2 indicates that more butanol is converted to 1-butene than is consumed in the consecutive reactions of 1-butene. Furthermore, 1-butene does not react in the gas phase or on bare ZrO_2 at 500 °C. On Al_2O_3 however, some conversion of pure 1-butene is initially observed and it increases slightly over time, possibly indicating the formation of active carbon species [42–44].

Fig. 3 shows the conversion of butyraldehyde at 500 °C in both pure and mixed feeds, for Rh/ZrO_2 as well as bare ZrO_2, bare Al_2O_3 and in the absence of catalyst. Initially on Rh/ZrO_2, Fig. 3A, the conversion of pure butyraldehyde is similar to 1-butene in Fig. 2A, i.e., lower than the conversion of butanol in Fig. 1A. Butyraldehyde conversion declines faster and more severely than either butanol or 1-butene. Curiously, the conversion curve of pure butyraldehyde over Rh/ZrO_2 in Fig. 3A is almost identical to the conversion curve on bare ZrO_2 in Fig. 3B. The conversion of butyraldehyde in the mixed feed is lower than pure butyraldehyde on bare ZrO_2 in Fig. 3B, reflecting the conversion of butanol to butyraldehyde. On Rh/ZrO_2 the conversion of butyraldehyde in the mixed feed is initially negative, indicating dehydrogenation of butanol into butyraldehyde

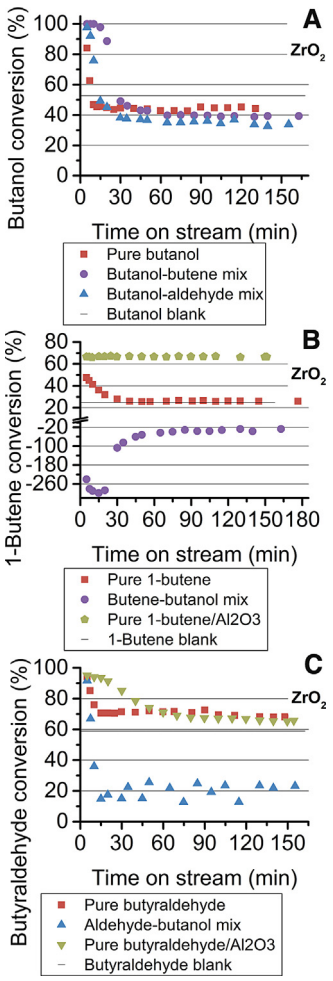

Fig. 4. Conversions at 700 °C. A) Butanol on ZrO_2, (B) 1-butene on ZrO_2 and $Al2O_3$ and (C) butyraldehyde on ZrO2 and Al2O3.

over Rh. However, as the Rh/ZrO_2 loses its capacity to produce butyraldehyde, the butyraldehyde conversion reaches the level observed on bare ZrO_2 in ca. 45 min and the level of pure butyraldehyde in ca. 120 min. On Al_2O_3, the conversion of butyraldehyde is initially lower than on bare ZrO_2, but remains stable, while the conversion over ZrO_2 decreases to a similar level.

3.2.2. Conversion at 700 °C

Conversions of butanol, 1-butene and butyraldehyde at 700 °C over bare ZrO_2 and Al_2O_3 are shown in Fig. 4. On the Rh/ZrO_2 catalyst the conversion is complete for all components (not shown). Any signs of deactivation are masked by the high conversion, except for pure butyraldehyde, the conversion of which starts to decline after 120 min on stream. On ZrO_2, the conversion of butanol in Fig. 4A collapses to blank level in the first 15 min, though the onset of the collapse is delayed by another ca. 15 min by the addition of 1-butene to the feed. Added butyraldehyde does not cause major changes to butanol conversion. Fig. 4B shows that the conversion of pure 1-butene is lower than the conversion of either butanol or butyraldehyde. It declines in ca. 30 min to blank level over ZrO_2, but remains stable over Al_2O_3. The conversion of 1-butene in the mixed feed is negative and shows an inverse trend compared to the conversion of butanol, due to dehydration of butanol into 1-butene. The conversion of pure butyraldehyde, Fig. 4C, approaches blank level over both ZrO_2 and Al_2O_3. However, the change takes ca. 10 min over ZrO_2, while on Al_2O_3 it takes 60 min. Similar to pure butyraldehyde, over ZrO_2 the conversion of butyraldehyde in the mixed feed declines rapidly, but more severely. The reduced conversion is most likely explained by the conversion of butanol into butyraldehyde in the gas phase, as will be shown later by the product distribution in blank experiments.

3.3. Product distributions

Table 1 shows the product distributions when reforming pure butanol over Rh/ZrO_2 and bare ZrO_2 at 500 and 700 °C at the start and the end of each experiment. Initially at 500 °C over the Rh/ZrO_2 catalyst, the major products are butenes, reforming products (carbon oxides and H_2) and butyraldehyde. Butenes make up roughly two thirds of the products with the ratio of 1-butene to other butenes 2:1. At 120 min, the only butene isomer observed is 1-butene, which makes up roughly half the known products, the rest of which consists equally of butyraldehyde and reforming products. The amount of unknown products is higher than in the blank experiment. This indicates that Rh catalyzes either the formation of unidentified species or the formation of precursors to the unidentified products. One likely component making up the unidentified products is *n*-butane; it could not be analyzed due to limitations of the analysis technique thermodynamically favored, as shown in Appendix A. At 700 °C over the Rh/ZrO_2 catalyst, only reforming products and a small amount of methane are observed. Over time, the changes in H_2, CO and CO_2 yields indicate water-gas-shift reaction pathway is deactivating. On bare ZrO_2 at 500 °C, the products at are primarily 1-butene, the yield of which slightly decreases over time, with a small amount of butyraldehyde and butyric acid also observed. At 700 °C, butenes are still the main product, although a small amount of reforming products are also present. The high yield of unidentified products originates in the gas phase at 700 °C, as seen in the blank experiment. After the rapid deactivation of ZrO_2 observed at 700 °C in Fig. 4A, the product distribution is sim-

Table 1
Product distribution in butanol SR initially and after 2 h operation. H_2 yield based on stoichiometric maximum, other products C_1-based. The yields of C2 and C3 components were negligible, and have been left out.

Catalyst	*T* (°C)	Time on stream (min)	Yield (%)											
			H_2	CO	CO_2	CH_4	Butanol	Butyraldehyde	Butyric acid	1-Butene	*Cis*-2-butene	*Trans*-2-butene	Isobutene	Unidentified
Rh/ZrO_2	500	7	13.5	13.6	3.6	0.3	22.6	10.3	1.7	24.6	1.5	1.8	11.2	8.9
		120	6.1	4.2	2.8	0.1	44.7	6.5	1.6	12.5	0.0	0,0	0.0	27.6
	700	5	74.6	43.2	56.8	2.5	0.0	0.0	0.0	0.0	0.0	0.0	0.0	0.0
		120	68.6	43.5	49.1	2.4	0.0	0.0	0.0	0.0	0.0	0.0	0.0	5.0
ZrO_2	500	5	0.3	0.0	0.3	0.0	51.4	5.0	1.6	37.3	0.0	0.0	0.0	4,3
		120	0.3	0.0	0.2	0.0	60.2	4.3	1.7	25.9	0.0	0.0	0.0	7.8
	700	5	6.5	4.7	4.9	3.0	15.9	4.6	0.0	27.7	0.0	9.0	0.1	30.1
		120	1.4	1.6	0.2	1.0	54.8	1.8	0.0	3,1	0.0	0.0	0.0	37.5
Blank	500	–	0.1	2.8	0.0	0.0	88.1	0.0	0.1	4.3	0.0	0.0	0.0	4.6
	700	–	2.3	4.7	0.3	1.0	47.3	2.4	0.6	6.6	0.9	0.0	0.0	36.0

Table 2
Product distribution in 1-butene SR initially and after 2 h operation. H_2 yield based on stoichiometric maximum, other products C_1-based. The yields of C2 and C3 components were negligible, and have been left out.

Catalyst	T (°C)	Time on stream (min)	Yield (%)											
			H_2	CO	CO_2	CH_4	Butanol	Butyraldehyde	Butyric acid	1-Butene	*Cis*-2-butene	*Trans*-2-butene	Isobutene	Unidentified
Rh/ZrO_2	500	5	9.1	9.0	3.6	0.2	0.0	0.0	0.0	48.0	11.7	22.8	0.0	4.3
		130	7.1	6.8	2.9	0.2	0.0	0.0	0.0	69.7	4.5	10.5	0,0	4.8
	700	7	69.7	31.3	62.7	1.3	0.0	0.0	0.0	0.0	2.1	0.0	0.0	2.5
		120	72.2	30.1	66.7	1.2	0.0	0.0	0.0	0.0	0.0	0.0	0.0	2.0
ZrO_2	500	5	0.1	0.1	0.0	0.0	0.0	0.0	0.0	99.6	0.0	0.0	0.0	0.3
		120	0.4	0.1	0.0	0.0	0.0	0.0	0.0	99.5	0.0	0.0	0.0	0.4
	700	5	1.3	0.5	0.5	1.2	0.0	0.0	0.0	52.4	17.1	8.7	0.0	19.4
		120	1.1	0.1	0.1	1.1	0.0	0.0	0.0	73.9	0.0	0.0	0.0	24.5
Al_2O_3	500	5	0.1	0.1	0.0	0.0	0.0	0.0	0.0	84.8	11.4	1.8	0.0	1.9
		130	0.4	0.3	0.0	0.1	0.0	0.0	0.0	75.3	18.0	7.4	0.0	0.0
	700	5	1.3	1.1	0.1	1.2	0.0	0.0	0.0	33.5	33.5	23.6	0.0	6.6
		130	1.2	0.5	0.1	1.2	0.0	0.0	0.0	33.9	34.3	27.0	0.0	2.6
Blank	500	–	0.2	0.2	0.0	0.0	0.0	0.0	0.0	99.5	0.0	0.0	0.0	0.3
	700	–	1.7	1.0	0.2	1.2	0.0	0.0	0.0	75.2	0.0	0.0	0.0	22.1

ilar to blank experiment, indicating complete deactivation of the ZrO_2 surface. These results have been reported in different form in our previous work [32].

Table 2 shows the product distributions during reforming of pure 1-butene over Rh/ZrO_2 and bare ZrO_2 and Al_2O_3 at 500 and 700 °C at the start and the end of each experiment. On the Rh/ZrO_2 catalyst at 500 °C, reforming products account for roughly a quarter of the 1-butene conversion, while the rest of the products are 2-butenes. *Trans*- and *cis*-2-butenes are formed in equilibrium ratio, as shown in Appendix A (Fig. A1). Deactivation of the catalyst over time affects the yields of all reaction products, but reforming product yields decrease proportionately less than 2-butene yields. At 700 °C only reforming is observed over the Rh/ZrO_2 catalyst. On bare ZrO_2 at 500 °C 1-butene is not converted significantly, whereas at 700 °C isomerization to 2-butenes is initially observed. The other products observed at 700 °C over bare ZrO_2 match blank experiments, suggesting origin in gas phase reactions. On bare Al_2O_3, only isomerization is observed at both 500 and 700 °C, as expected [45]. However, the ratio of the 2-butene isomers over both bare oxides is different from the equilibrium ratio, surprisingly. It should also be noted that the yield of unidentified products at 700 °C is small over both Rh/ZrO_2 and Al_2O_3, whereas over bare ZrO_2 their yield is at the level of blank experiments.

Table 3 shows the product distributions during reforming of pure butyraldehyde over Rh/ZrO_2 and bare ZrO_2 and Al_2O_3 at 500 and 700 °C at the start and the end of each experiment. Initially on the Rh/ZrO_2 catalyst at 500 °C, butenes and reforming products are observed at roughly equal yields. However, the ratio of hydrogen to carbon oxides is lower than observed during the reforming of butanol and 1-butene, indicating consumption of hydrogen in side reactions. Both the reforming and butene yields suffer equally from the deactivation of the catalyst. The rate of decline (not shown) of the butene and reforming yields is also equal. At 700 °C, the main reaction over Rh/ZrO_2 is reforming, with only very low amounts of butenes and a significant yield of unidentified products observed. On bare ZrO_2 the products are mostly unidentified with yields much higher than blank at both 500 and 700 °C. At 700 °C, the total yield of reforming products is similar to blank experiment, but the initial higher yields for CO_2 and H_2 show that ZrO_2 catalyzes WGS to a small extent, which has been reported elsewhere [46]. On bare Al_2O_3, at 500 °C there is only a low but steady yield of butenes and butyric acid, whereas at 700 °C the main products are unidentified and decomposition products. Butenes are only formed after deactivation of the catalyst. The formation of unidentified products over the bare oxides declines severely over time, approaching the yield observed in blank reactor. This suggests that the majority of unidentified products are formed catalytically.

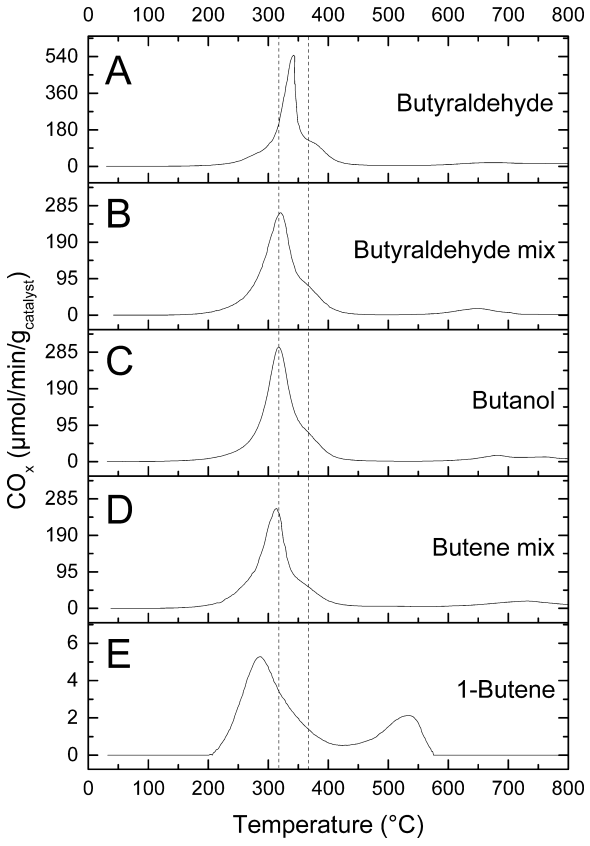

Fig. 5. TPO of spent Rh/ZrO_2 catalysts after SR at 500 °C. The two main peaks are indicated by a dashed line. Graphs from butyraldehyde and 1-butene reforming have different scale.

3.4. Characterization of spent Rh/ZrO_2

The TPO graphs of the Rh/ZrO_2 catalysts spent at 500 °C are shown in Fig. 5. The corresponding graphs for the bare ZrO_2 are shown in Appendix B (Fig. B1). For easier comparison, the TPO graphs in Fig. 5 are shown partially magnified in a single graph in Appendix B (Fig. B3). The TPO graphs of the deposits from reforming of pure and mixed butanol (Fig. 5B–D) show a sharp main peak at ca. 315 °C, a shoulder at 370 °C and some secondary peaks above 600 °C. In the case of butyraldehyde reforming deposits (Fig. 5A), the main peak is more intense and located at 340 °C, and there is a low shoulder below 300 °C. The CO_2 signal observed during TPO

Table 3
Product distribution in butyraldehyde SR initially and after 2 h operation. H_2 yield based on stoichiometric maximum, other products C_1-based. The yields of C2 and C3 components were negligible, and have been left out.

Catalyst	T (°C)	Time on stream (min)	Yield (%)											
			H_2	CO	CO_2	CH_4	Butanol	Butyraldehyde	Butyric acid	1-Butene	*Cis*-2-butene	*Trans*-2-butene	Isobutene	Unidentified
Rh/ZrO2	500	6	12.8	18.5	4.0	0.6	0.0	47.1	3.7	18.7	1.5	1.5	0.0	4.3
		120	4.2	3.2	3.0	0.2	0.0	69.8	3.1	7.7	0.0	0.0	0.0	12.8
	700	5	60.9	24.9	52.2	3.4	0.0	0.0	0.0	0.0	0.9	0.0	0.0	18.5
		122	53.7	36.6	36.3	5.4	0.0	0.1	0.0	1.4	1.3	0.0	0.0	18.8
ZrO2	500	5	0.8	0.2	0.7	0.1	1.6	54.9	3.2	3.2	0.0	0.0	0.0	36.0
		130	0.7	0.2	0.6	0.1	1.6	75.7	3.2	3.2	0.0	0.0	0.0	15.3
	700	5	7.5	4.3	6.6	3.5	0.0	5.6	0.8	0.0	2.7	0.0	3.9	72.5
		130	1.8	7.4	0.3	4.8	0.0	30.8	4.5	3.0	1.5	0.0	0.0	47.4
Al2O3	500	5	0.1	2.3	0.2	0.1	0.0	76.6	3.2	8.7	1.6	0.0	0.0	7.1
		120	0.0	2.4	0.2	0.1	0.0	81.9	3.2	8.9	1.6	0.0	0.0	1.5
	700	5	4.1	9.2	2.7	3.9	0.0	5.0	0.0	0.0	0.0	0.0	0.0	79.1
		120	2.5	11.8	0.1	4.8	0.0	33.2	0.0	7.8	6.6	0.0	0.0	35.5
Blank	500	–	0.0	2.2	0.0	0.1	0.0	90.3	1.6	1.4	0.0	0.0	0.0	4.2
	700	–	2.0	10.5	0.1	5.0	0.0	41.1	1.6	2.1	0.5	0.0	0.0	38.9

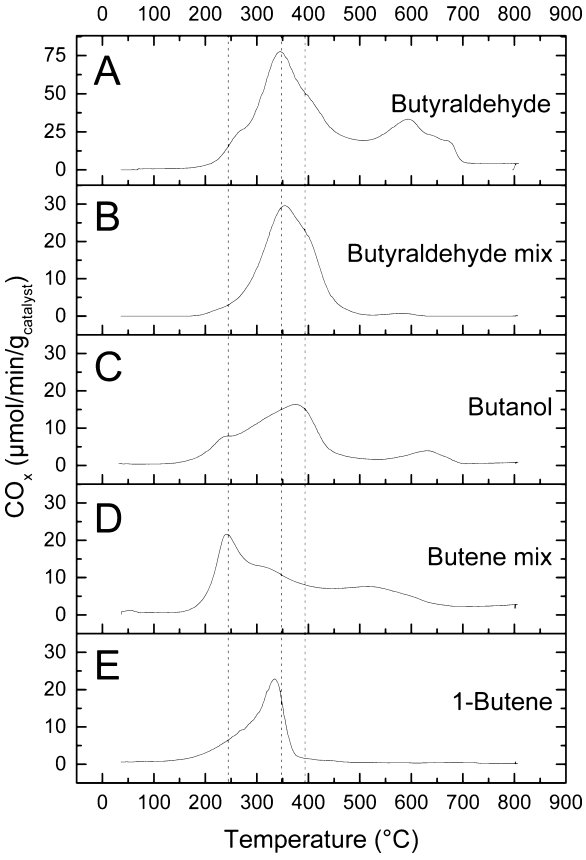

Fig. 6. TPO of spent Rh/ZrO_2 catalysts after SR at 700 °C. The three main peaks are indicated by a dashed line. The graph from butyraldehyde reforming has a different scale.

of 1-butene reforming deposits is very low in comparison to the deposits formed from other feeds, and shows a main peak at 285 °C with a low shoulder at 330 °C and a second peak at 525 °C. The TPO graphs of the Rh/ZrO_2 catalysts spent at 700 °C are shown in Fig. 6. The corresponding graphs for the bare ZrO_2 are shown in Appendix B (Fig. B2). The butanol and butanol-butene mix reforming deposits (Fig. 6C and D, respectively) show two overlapping peaks at 240 °C and 320–370 °C. Pure and mixed butyraldehyde reforming deposits (Fig. 6A and B, respectively) show a sharp peak at ca. 350 °C in addition to the peaks observed with butanol. 1-butene reforming deposits (Fig. 6E) show a sharp peak at 330 °C with a wide shoulder at 275 °C.

Table 4 shows the results of the elemental analysis of the coked catalyst samples. There was some remaining SiC filler in the coked samples, which interfered with the carbon content analysis during elemental analysis. However, the effect of the SiC should be minimal in the oxygen and hydrogen analysis. Therefore, the composition of the deposits is calculated using the C content measured with TPO and the H and O content from the elemental analysis. Even though the samples for TPO and CHNS + O are different, the reaction experiments preceding the analysis were done following identical procedure and conditions. In Table 4, a significant amount of oxygen is observed in the deposits on Rh/ZrO_2 formed during butanol and butyraldehyde reforming at 500 °C. The very low amount of deposition during 1-butene reforming over Rh/ZrO_2 at 500 °C made the elemental analysis results unreliable, and they are left out of the discussion. At 700 °C, the amount of coke is clearly the highest in the deposits formed out of butyraldehyde, while the deposits formed out of butanol and 1-butene are similar, both in quantity and composition. In contrast, on bare ZrO_2 the highest oxygen content is observed from butanol reforming at both temperatures, while the highest carbon content is observed from butyraldehyde, and the composition of the butyraldehyde and 1-butene deposits are nearly identical, especially at 700 °C.

4. Discussion

4.1. Reaction network

4.1.1. Butanol reforming

In our previous work [32], based on the observed product distributions a schematic reaction network was proposed for the steam reforming of butanol, shown in Fig. 7. The reaction to CO and H_2 is thought to proceed through three alternative routes. First is directly from butanol on the Rh particles (reaction 1). Second and third are through intermediates: 1-butene formed by dehydration on acid sites (reactions 2 and 3) or butyraldehyde formed by dehydrogenation on the Rh or basic sites (reactions 6 and 7). Of these, formation of 1-butene is clearly the dominant intermediate product at temperatures below 700 °C [32]. Both intermediates in turn have possible side reactions, which may or may not contribute to carbon deposition and deactivation of the catalyst. The partial reaction schemes for 1-butene and butyraldehyde reforming are further discussed below in Figs 8 and 9, respectively. This will be discussed based on the data obtained at 500 °C as it is not possible to do the same at 700 °C, because of the full conversion to reforming products. However, it is reasonable to assume that the reaction

Table 4
The amount of deposited carbon on coked Rh/ZrO_2 and ZrO_2 samples according to TPO and the CHO-composition of the deposits, according to TPO and CHNS + O analysis.

Catalyst	Reactant	Temperature (°C)	C deposits TPO (wt.%)	Deposit composition (mol.%)		
				C	H	O
Rh/ZrO_2	Butanol	500	5.3	87	9.4	3.4 ± 0.4
	Butyraldehyde		8.1	84	12	4.0 ± 1.6
	1-butene		0.2	N/A	N/A	N/A
	Butanol	700	0.9	74	23	3.0 ± 2.1
	Butyraldehyde		4.0	86	10	3.8 ± 0.7
	1-butene		0.6	68	29	3.4 ± 1.4
ZrO_2	Butanol	500	1.3	71	24	5.5 ± 2.9
	Butyraldehyde		2.5	79	19	2.2 ± 0.4
	1-butene		0.8	80	19	0.5 ± 0.4
	Butanol	700	2.8	78	17	4.6 ± 0.1
	Butyraldehyde		3.9	90	8.9	1.2 ± 0.8
	1-butene		3.2	85	13	1.5 ± 0.6

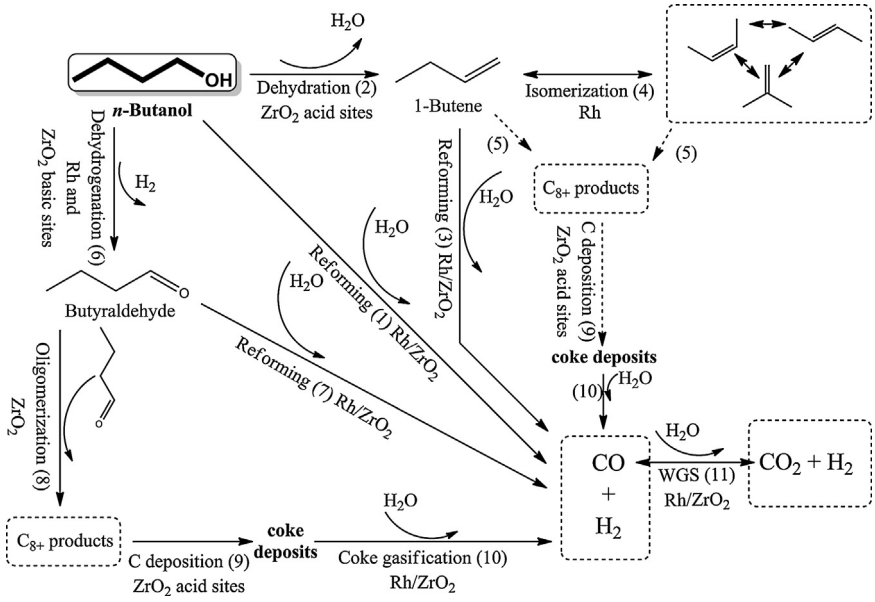

Fig. 7. Schematic reaction network for steam reforming of *n*-butanol. [32].

pathways at 500 °C are also involved in the reaction occurring at 700 °C.

4.1.2. 1-butene reforming

Based on the product distributions presented in Table 2, the main reaction of 1-butene at 500 °C is isomerization (Fig. 8, reaction 1). This can be either hydroisomerization catalyzed by Rh [47] using the hydrogen naturally provided through the reforming reaction, or isomerization catalyzed by strong acidic surface sites[45]. This agrees with the observation that isomerization is observed on both Rh/ZrO_2 and Al_2O_3 (Table 2), but not on bare ZrO_2 at 500 °C. Steam reforming of butenes (reaction 2) is slow compared to isomerization at 500 °C, reforming products accounting for ca. 25% of the reaction products of butenes. Hydrogenation of butenes to butane (Fig. 8, reaction 8) might explain in part the high amount of unidentified products observed in butanol reforming at 500 °C (Table 1). Thermodynamics at 500 °C (Appendix A, Fig. A1) favor the hydrogenation reaction. However, butane cannot be detected with the analysis techniques used. Oligomerization of olefins to polyaromatic deposits on acid sites (Fig. 8, reactions 4 and 5) and the gradual carbonization of those deposits to graphite (Fig. 8, reaction 7) is well documented [42,43] and sometimes claimed as the primary mechanism to carbon deposition from alcohols [8,48]. However, this is minor under the reaction conditions employed, especially on ZrO_2, based on the very low carbon deposition from 1-butene observed with TPO in the present work (ZrO_2 in Fig. 11 and Al_2O_3 in Appendix B, Fig. B7).

4.1.3. Butyraldehyde reforming

The reaction network for butyraldehyde reforming (Fig. 9) is much more complex as compared to 1-butene (Fig. 8). Based on the product distribution in Table 3, at 500 °C the yields of butenes and reforming products are similar. The butene yield is likely explained via dehydration of butanol (Fig. 9, reaction 6). The butanol is in turn formed through both hydrogenation of butyraldehyde (Fig. 9, reaction 3) as well as hydrolysis of butyl butyrate formed in Tischenko esterification (Fig. 9, reaction 4). The latter, catalyzed by acidic surface sites [49], is supported by the detection of butyric acid and butyl butyrate in the condensate. However, the relatively low hydrogen yield as compared to the carbon oxide yields, observed in Table 3, and the relatively small amounts of butyric acid and butyl butyrate, indicate that hydrogenation followed by dehydration is probably to dominant pathway to butene. Even though Rh has been used in hydrodeoxygenation (HDO, Fig. 9, reaction 7) [50], the atmospheric pressure and much higher temperatures used in this study, and the tendency of Rh towards decarbonylation instead

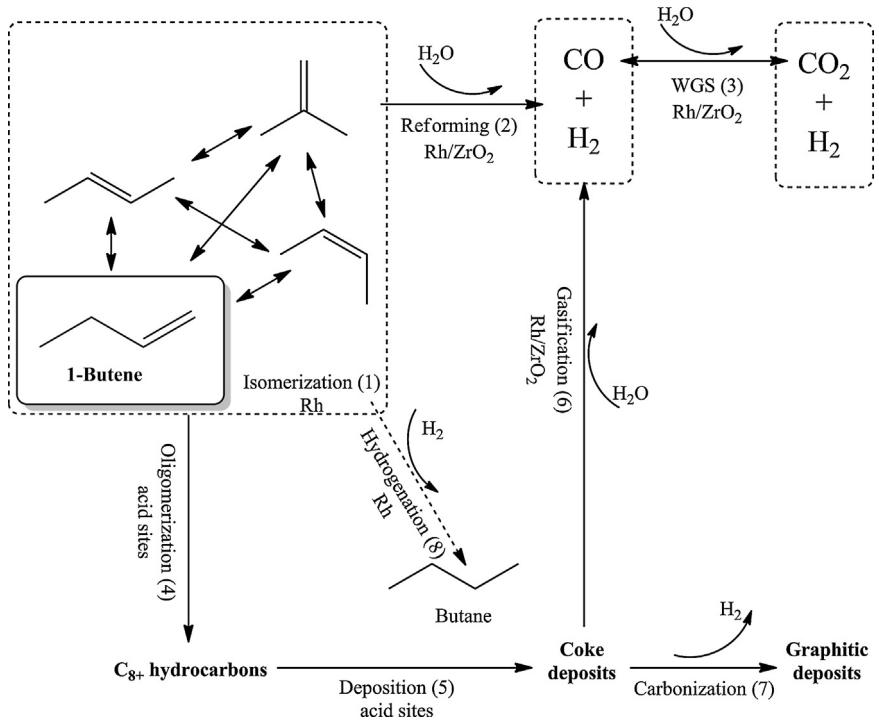

Fig. 8. Schematic reaction network for steam reforming of 1-butene.

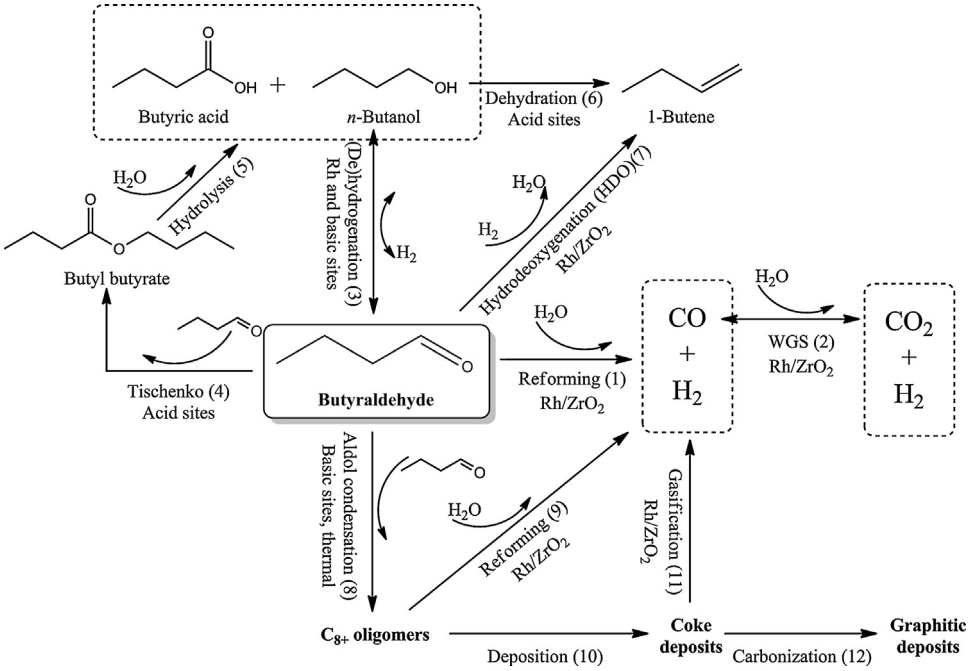

Fig. 9. Schematic reaction network for steam reforming of butyraldehyde. Further reactions of butanol and 1-butene are omitted for clarity.

of hydrodeoxygenation/hydrogenolysis, make the direct pathway seem unlikely. The reforming of butyraldehyde mostly proceeds through the direct route (Fig. 9, reaction 1). Reforming of butanol and butenes make only a minor contribution, based on a comparison of the product yields, as will be discussed later. Reforming of butyraldehyde oligomers (Fig. 9, reaction 9) is likely to contribute as well, based on the yield of unidentified products increasing with the deactivation of the catalyst, but the contribution is probably minor.

A remarkably high yield of unidentified products is observed in butyraldehyde reforming, particularly over the bare oxides. This suggests that these are mostly oligomers of butyraldehyde formed via a combination of aldol and Tischenko reactions (Fig. 9, reactions 8 and 4, respectively), both of which are known to be catalyzed by oxide materials [49,51,52]. Butyl butyrate from the Tischenko reaction hydrolyzes readily [49] and the yield of butyric acid is never particularly high, which suggests that aldol condensation is the main oligomerization pathway. The high yield of unidentified products in the blank experiments at 700 °C suggests that the oligomers are also formed through gas phase reactions at high temperatures. In our previous work, we tentatively linked carbon deposition on the support to the oligomerization of butyraldehyde

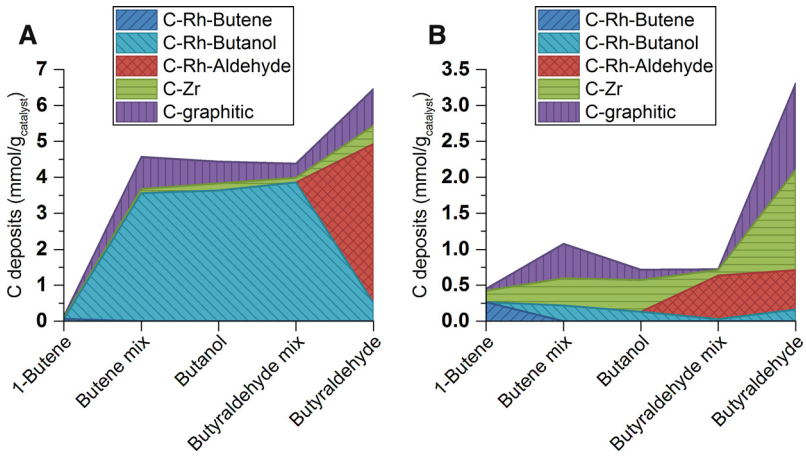

Fig. 10. The amounts of deposited carbon on the Rh/ZrO_2 catalyst at (A) 500 °C and (B) 700 °C.

[32], and similar has been suggested for ethanol reforming [53]. The present findings support the hypothesis. The high yield of unidentified products (Table 3) coincides with the large amount of deposited carbon (Table 4), especially at 700 °C. At 700 °C Rh/ZrO_2 is capable of reforming the oligomers (Fig.e 9, reaction 9) to some extent, while the oxides without Rh are overwhelmed and deactivate rapidly, as is seen in Fig. 4A, B, and C.

4.1.4. Deposited coke species

The peaks on TPO of carbonaceous deposits that form during reforming at 500 °C of pure and mixed butanol (Fig. 5B, C and D) are assigned as discussed in our previous work [32]. The main peak at 315–340 °C is assigned to deposits on/near Rh particles, hereafter labeled C_{Rh}. Furthermore, we propose that butanol, butane and butyraldehyde cause deposition of different carbonaceous species with different reactivity on/near Rh particles, hereafter labeled $C_{Rh\text{-}butanol}$, $C_{Rh\text{-}butene}$ and $C_{Rh\text{-}aldehyde}$. This is based on the onset temperatures of the oxidation peaks after reforming at 500 °C shown in Appendix B (Fig. B3), from which three observations are made. First, the low temperature shoulder (below 300 °C) observed after butyraldehyde reforming (Fig. 5A) corresponds to the $C_{Rh\text{-}butanol}$ peak in Fig. 5B, C and D, as the rate of formation of CO_x is identical for all butanol containing feed-compositions on Rh/ZrO_2 up to 270 °C (Appendix B, Fig. B3); the exact peak temperature cannot be observed because of the low intensity of the shoulder as compared to the much higher intensity of main peak at higher temperature. Second, the intense main peak observed at 340 °C after butyraldehyde reforming corresponds to a species originating from butyraldehyde, i.e., $C_{Rh\text{-}aldehyde}$. Third, the onset temperature of the first peak observed after 1-butene reforming is higher than the other feeds (Appendix B, Figs. B3 and B4), indicating $C_{Rh\text{-}butene}$ is also a different species with lower reactivity. The shoulder around 370 °C (Fig. 5), which corresponds to main peak of TPO of bare ZrO_2 samples (Appendix B, Fig. B1), is assigned to reactive deposits on the support, hereafter labeled C_{Zr}. The deposits oxidized above 600 °C are considered to be graphitic in nature and are thus labeled $C_{graphitic}$.

The TPO results after reforming at 700 °C (Fig. 6) follow the same designations. The peaks/shoulders at 240 °C correspond to $C_{Rh\text{-}butanol}$ and $C_{Rh\text{-}butene}$, although the exact temperature of the $C_{Rh\text{-}butene}$ shoulder is hard to pinpoint due to its low and wide shape. The peaks/shoulders corresponding to C_{Zr} are located at ca. 370 °C. The C_{Zr} peak/shoulder observed after pure and mixed 1-butene reforming are shifted to 330 and 320 °C, respectively. These are assigned to C_{Zr} based on comparison with the corresponding TPO graphs on bare ZrO_2 of the peaks (Appendix B, Fig. B2) and the onset temperatures (Appendix B, Fig. B5), in which the shift is also visible. The main peak observed from pure and mixed butyraldehyde is the $C_{Rh\text{-}aldehyde}$ peak at 350 °C.

Based on elemental composition of the deposits in ZrO_2 in Table 4, the C_{Zr} deposits originating from butanol are oxygen rich, while the C_{Zr} deposits from butyraldehyde and 1-butene are oxygen poor. Therefore, most of the oxygen content of the deposits from butanol on Rh/ZrO_2 is probably in the C_{Zr} species, whereas most

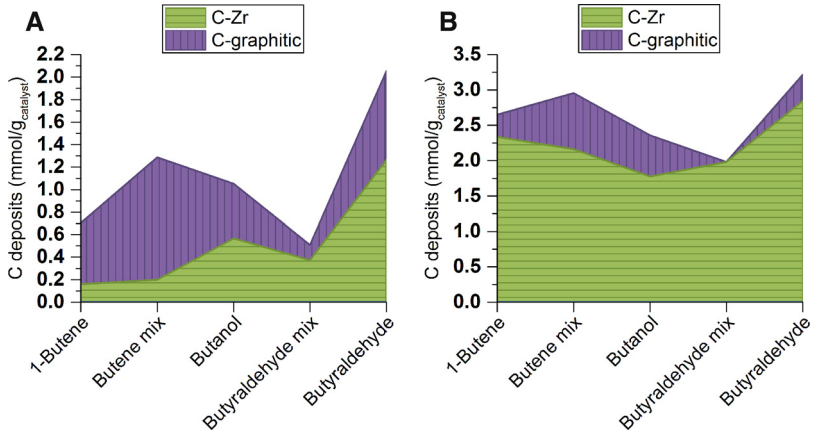

Fig. 11. The amounts of deposited carbon on the bare ZrO_2 at (A) 500 °C and (B) 700 °C.

of the oxygen content of the deposits from butyraldehyde is in the $C_{Rh\text{-}aldehyde}$ species. Possibly, two different C_{Zr} species, one originating from butanol and one from butane and butyraldehyde, are present in all samples but the limited resolution of the TPO peaks is insufficient to observe this directly.

Deconvolution of the peaks was carried out with OriginPro 9.1 software. The number of peaks is chosen according the discussion above and the initial positions were assigned manually and fitted to Gaussian, Lorentz or Gaussian_LorenCross functions, depending on their shape. The fitting allowed optimization of both the position and intensity of all peaks, in order to improve the fit to the experimental data. Two examples of deconvolution results are shown in Fig. B6 in Appendix B. Based on the ratios of the surface areas of the fitted peaks, the amounts of the different types of carbon deposits were calculated and are shown in Fig. 10 for the Rh/ZrO_2 catalyst and in Fig. 11 for the bare oxides. On Rh/ZrO_2 at 500 °C, Fig. 10A, it is clear that at 500 °C butanol and butyraldehyde cause coke deposition while deposition from 1-butene is minor. Butyraldehyde reforming results in the largest quantity of coke deposits in both temperatures. On bare ZrO_2, Fig. 11A and B, the amounts of deposited carbons are very similar for all feeds, except for the feeds containing butyraldehyde. At both temperatures, reforming of pure butyraldehyde results in the highest amount of deposits and butyraldehyde butanol mixture the lowest amount of deposits, surprisingly. This indicates that the deposition processes are not linear as a function of the intermediate product concentrations. Further study would be needed to explain this unexpected observation. At 700 °C on Rh/ZrO_2 (Fig. 10B), the amounts of $C_{Rh\text{-}butanol}$ and $C_{Rh\text{-}butene}$ are very low whereas the amount of $C_{Rh\text{-}aldehyde}$ is high even with a small addition of 10 mol.% butyraldehyde to the feed. On bare Al_2O_3 (Appendix B, Fig. B7), the amounts of carbon from pure 1-butene are slightly higher than on ZrO_2 in Fig. 11. The amounts of carbon deposited from pure butyraldehyde, however, are nearly 10 times as high on Al_2O_3 as on ZrO_2.

4.2. Reaction mechanism, network and deactivation

In butanol reforming at 500 °C, most of the deposited coke is $C_{Rh\text{-}butanol}$ and only a little is deposited on the support as is easily seen in Figs. 10A and 11A. Conversely, at 700 °C (Figs. 10B and 11B) most of the deposits are C_{Zr} and the deposited quantity is higher on the bare oxides. Coupled with the observed deactivation behavior of the catalyst at 500 C and 700 C (Fig. 1 and 4), it becomes apparent that the deactivation of the reforming reactions is caused by the accumulation of carbon on and near the Rh particles. The amount and type of carbon deposited at 500 °C on the Rh/ZrO_2 suggests that this formation happens on the Rh particles directly, instead of deposits on the support encroaching on the particles. The repeat experiments with TPO regenerated catalyst (not shown) revealed no difference between fresh and regenerated catalyst, indicating that deactivation via sintering of Rh particles does not occur significantly in the time scale of these experiments.

In our previous work [32], a mechanism was proposed for the formation of the C_{Rh} species in butanol reforming, shown in Fig.12. Similar mechanisms have been proposed for the reforming of alkanes [34] and other oxygenates [16] on various different catalyst systems. The reactants form surface species on the Rh particles, which then either decompose into syngas through reforming reactions with surface hydroxyls formed from steam, either on the support [16] or directly on Rh, or form carbon deposits via C-C coupling. Coke formation on the Rh particles is therefore simply the result of the ratio between the rate of formation and the rate of reforming of the surface species. At 500 °C, reforming is not fast enough and the catalyst is overwhelmed. Based on the almost complete lack of C_2 and C_3 products, it is apparent that the rate of the reforming surface reactions is controlled by the initial step of

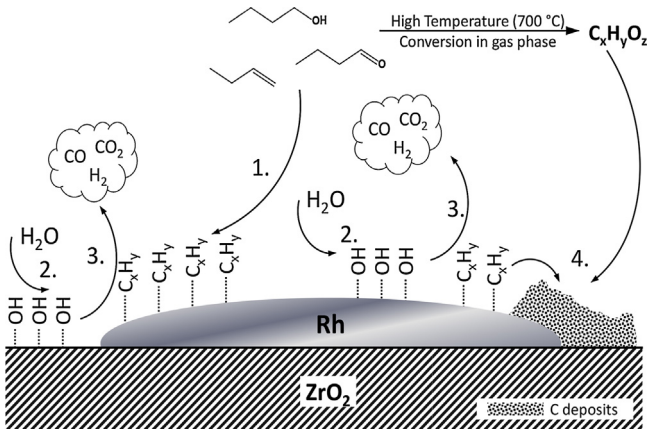

Fig. 12. Proposed surface reaction mechanism. Step 1: formation of surface species. Step 2: water activation, both on the support and on Rh. Step 3: steam reforming reactions. Step 4: coke deposition from surface species or gas phase (at high temperature).

decomposing C_4 into smaller fragments. The reforming reactions at 500 °C are likely limited by the steam activation step [22,23], which can be enhanced by either increasing the S/C ratio [28,29] or by modifying the catalyst support [24]. At 700 °C, the presence of Rh clearly reduces the formation of coke species on the support (Figs. 10 and 11). This most likely happens via rapid reforming of the coke precursor surface species and/or coke reforming via hydroxyl spill-over from zirconia to Rh.

Based on our previous work, the role of intermediate products in the deactivation process was unclear. The present work brings more insight to this matter. It is clear, that under the reaction conditions used in this study 1-butene contributes very little to coke deposition on both Rh and ZrO_2 when compared to butanol or butyraldehyde (Fig. 10). Butyraldehyde does not only cause more deposition than butanol, but the $C_{Rh\text{-}aldehyde}$ species is capable of accumulating on the catalyst even at 700 °C. This means that suppression of the dehydrogenation pathway, via butyraldehyde, might be beneficial for the coking resistance of the catalyst. This could be achieved by modification of the support, the active metal or both, e.g. by optimizing the acid-base properties of the support with additives.

A comprehensive reaction network including all the major reaction and coke deposition pathways, combining the data of the individual networks for butanol, 1-butene and butyraldehyde is presented in Fig.13. Estimation of the exact contributions of each of the three different pathways to reforming activity, i.e. direct reforming, via dehydration and via dehydrogenation, would require working out the detailed kinetics for the system. However, based on the conversions and product distributions of the three different pure feeds (Tables 1–3), it is possible to estimate rough ratios of the contributions of the three pathways. The dehydration reaction (Fig. 13, reaction 2) is fast and thermodynamically favored (Appendix A), but the rate of butene reforming (Fig. 13, reaction 4) at 500 °C is slow. In contrast, butyraldehyde is reformed (Fig. 13, reaction 6) rapidly when compared to butanol and 1-butene, but the dehydrogenation (Fig. 13, reaction 5) is slow. Direct reforming (Fig. 13, reaction 1) is limited at 500 °C, but has a relatively larger impact per reacted mole. The result is that at 500 °C all three pathways contribute roughly equally to the reforming yield. As reforming reactions become faster with increasing temperature, reforming of the main intermediate, 1-butene, becomes the most important reforming pathway at 700 °C, assuming that the ratio of the direct reforming, dehydration and dehydrogenation reactions (Fig. 13, reactions 1, 2 and 5, respectively) is about constant. Although mass transfer does not affect the reaction pathways them-

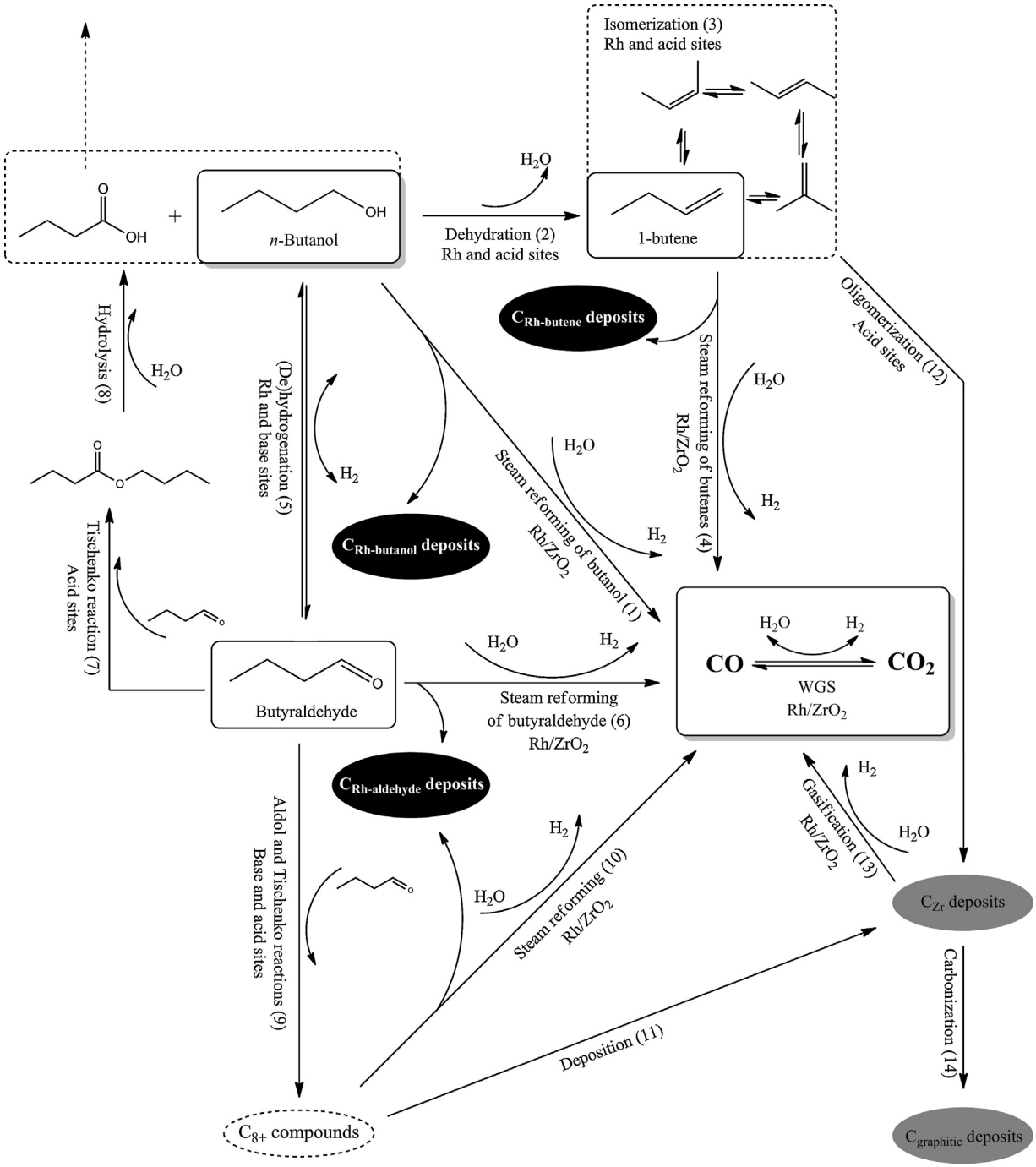

Fig. 13. Comprehensive reaction network for butanol reforming, including deactivation pathways.

selves, it is likely to affect the ratio of the pathways. However, without detailed investigation into either kinetics or the effect of mass transfer, it is not possible to estimate the effect of diffusion limitations on the product distribution.

The C_{Rh} deposits are mostly formed as a byproduct of either the direct butanol reforming pathway ($C_{Rh\text{-}butanol}$ Fig. 13, reaction 1) or either butyraldehyde or butyraldehyde oligomer reforming ($C_{Rh\text{-}aldehyde}$ Fig. 13, reactions 6 and 10, respectively); and to a much smaller extent via butene reforming (Fig. 13, reaction 4). The origin of the C_{Zr} species also seems to be the butyraldehyde pathway. This is based on the relatively low amounts deposited from 1-butene compared to butyraldehyde on the bare ZrO_2 (Fig. 10). The possible gasification of the deposits (reaction 13) is only active at high temperatures, where hydroxyl groups on zirconia and/or Rh are able to keep the overall deposition low. The carbonization reaction (reaction 14) is slow, only becoming significant after prolonged reaction times, as observed in our previous work [32].

5. Conclusions

Reaction schemes were presented for steam reforming of butanol and the two intermediate products: 1-butene and butyraldehyde. Butanol reforming scheme was updated accordingly to also include the coke formation pathways. At lower temperatures, butenes mainly undergo isomerization reactions, while reforming is slow. Butyraldehyde has a complex reaction

network, including coupling reactions and formation of butenes via butanol. The rate of direct steam reforming of the individual components decreases in the order butyraldehyde > butanol > 1-butene. At 500 °C, all three pathways, i.e. direct reforming, via dehydration and via dehydrogenation, contribute roughly equally to total reforming of butanol. Formation of coke deposits can be described by five types of coke species: $C_{Rh\text{-}butanol}$, $C_{Rh\text{-}butene}$, $C_{Rh\text{-}aldehyde}$, C_{Zr} and $C_{graphitic}$; the different C_{Rh} species reveal distinct differences in their reactivity in TPO. C_{Zr} species were mostly formed via butyraldehyde oligomers acting as precursors. The catalyst deactivates by deposition of the various C_{Rh} species on/near the Rh particles. The deposition is a side reaction of the reforming surface reaction and the rate by reacting component decreases in the order butyraldehyde > butanol » 1-butene.

Acknowledgements

Financial support from the Finnish Funding Agency for Technology and Innovation (Tekes) and from Neste Oil is acknowledged. We thank Dr. Kristiina Uusi-Esko for the XRF measurements, Arto Mäkinen for the chemisorption measurements, and Atte Mikkelson and Ulla Vornamo (VTT) for the elemental analysis measurements. Irene Coronado Martín, Miriam Cuadrado Martin and Markus Hovi are thanked for their help in performing a part of the reaction experiments.

Appendix A.

Thermodynamic calculations

Fig. A1A shows the thermodynamic equilibrium of the C_4 species

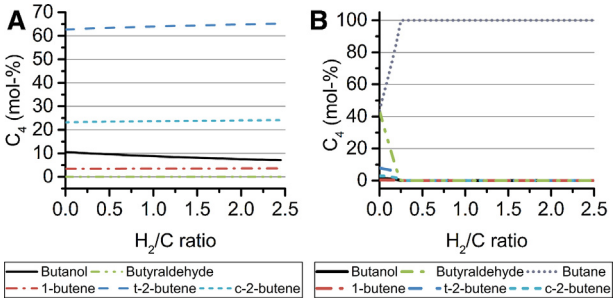

Fig. A1. Thermodynamic equilibrium of the C4 species as a function of H2/C ratio at 500 °C with S/C ratio 4. (A) *n*-butane not considered. (B) n-butane considered.

as a function of H_2/C ratio at 500 °C with S/C ratio 4, calculated with the HSC Chemistry 6.12 software [54] based on Gibbs free energy minimization. The equilibrium is heavily on the side of 2-butenes, formed in 3:1 trans:cis ratio. Isobutene was considered in the calculations, but its yield was zero. As shown in Fig. A1B, considering butane in the calculation switched the equilibrium completely to butane, as long as sufficient hydrogen was present.

Appendix B.

Additional TPO data

Characterization of spent bare ZrO_2

See Figs. B1 and B2.

TPO peak allocation

See Figs. B3–B5.

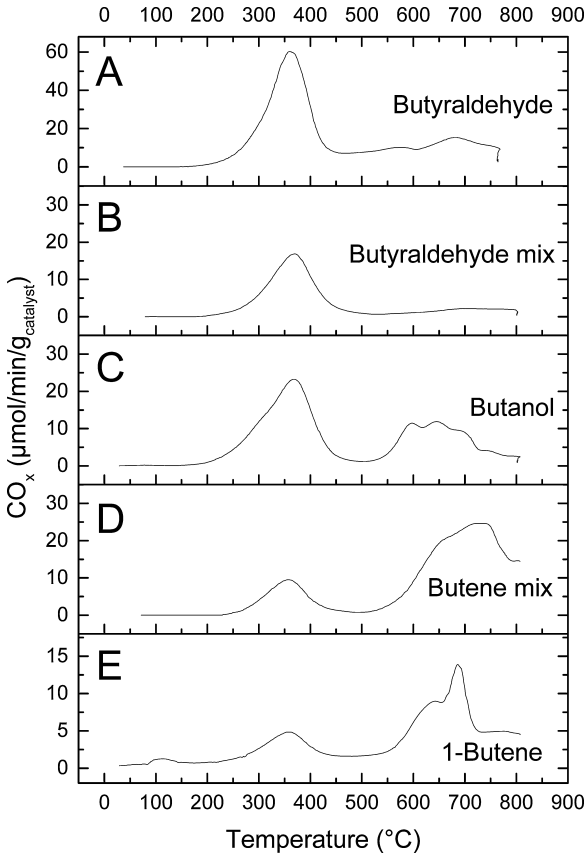

Fig. B1. TPO of spent bare ZrO2 catalysts after SR at 500 °C.

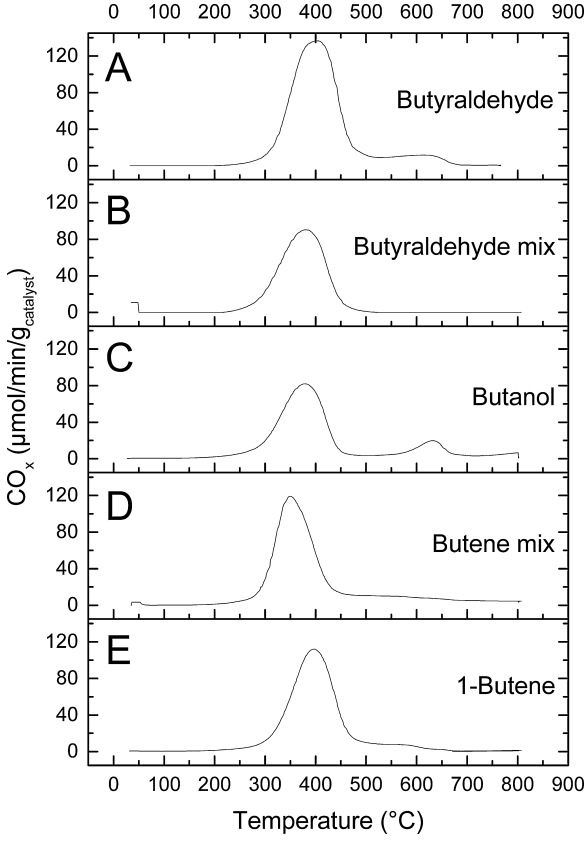

Fig. B2. TPO of spent bare ZrO2 catalysts after SR at 700 °C.

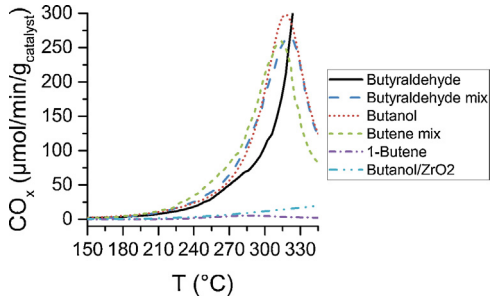

Fig. B3. Overlapping TPO graphs from reforming with Rh/ZrO2 at 500 °C. A close-up on 150–350 °C.

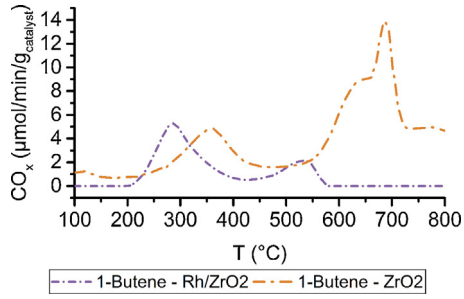

Fig. B4. Comparison of TPO graphs from 1-butene SR over RH/ZrO2 and bare ZrO2 at 500 °C.

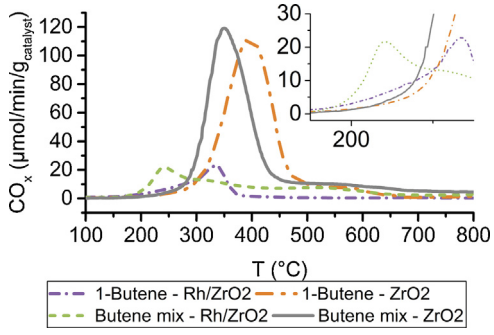

Fig. B5. Comparison of TPO graphs from mixed and pure 1-butene SR over Rh/ZrO_2 and bare ZrO_2 at 700 °C. Close-up of 150–350 °C included.

TPO graph deconvolution

See Fig. B6.

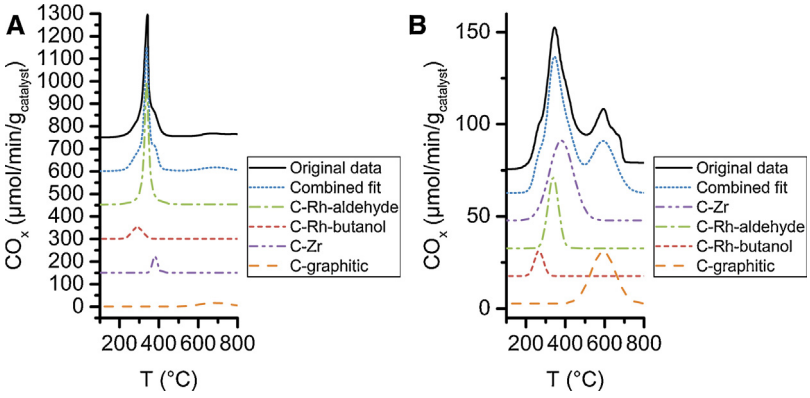

Fig. B6. Example of the deconvolution of the TPO graphs using OriginPro 9.1. The original data, the fitted peaks and the combined fit peak are shown stacked by base line offset. (A) Butanol-butyraldehyde mix SR over Rh/ZrO_2 at 500 °C. (B) Butyraldehyde SR over Rh/ZrO_2 at 700 °C.

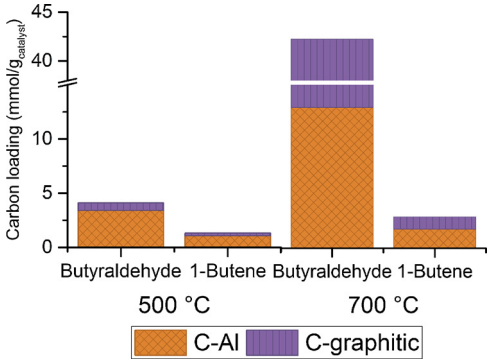

Fig. B7. Total carbon loadings observed on spent Al_2O_3.

Coke deposition on Al_2O_3

See Fig. B7.

References

[1] J.D. Holladay, J. Hu, D.L. King, Y. Wang, An overview of hydrogen production technologies, Catal. Today 139 (2009) 244–260, http://dx.doi.org/10.1016/j.cattod.2008.08.039.

[2] D. Wang, S. Czernik, D. Montané, M. Mann, E. Chornet, Biomass to hydrogen via fast pyrolysis and catalytic steam reforming of the pyrolysis oil or its fractions, Ind. Eng. Chem. Res. 36 (1997) 1507–1518, http://pubs.acs.org/doi/abs/10.1021/ie960396g (accessed 27.02.15.

[3] R. Garcia, S. French, E. Czernik, Catalytic steam reforming of bio-oils for the production of hydrogen: effects of catalyst composition, Appl. Catal. A Gen. 201 (2000) 225–239, http://dx.doi.org/10.1016/S0926-860X(00)440-3.

[4] M. Ni, D.Y.C. Leung, M.K.H. Leung, A review on reforming bio-ethanol for hydrogen production, Int. J. Hydrogen Energy 32 (2007) 3238–3247, http://dx.doi.org/10.1016/j.ijhydene.2007.04.038.

[5] M. Benito, R. Padilla, L. Rodríguez, J.L. Sanz, L. Daza, Zirconia supported catalysts for bioethanol steam reforming: Effect of active phase and zirconia structure, J. Power Sources 169 (2007) 167–176, http://dx.doi.org/10.1016/j.jpowsour.2007.01.047.

[6] A. Gutierrez, R. Karinen, S. Airaksinen, R. Kaila, A.O.I. Krause, Autothermal reforming of ethanol on noble metal catalysts, Int. J. Hydrogen Energy 36 (2011) 8967–8977, http://dx.doi.org/10.1016/j.ijhydene.2011.04.129.

[7] A. Le Valant, A. Garron, N. Bion, F. Epron, D. Duprez, Hydrogen production from raw bioethanol over Rh/$MgAl_2O_4$ catalyst, Catal. Today 138 (2008) 169–174, http://dx.doi.org/10.1016/j.cattod.2008.06.013.

[8] A. Le Valant, A. Garron, N. Bion, D. Duprez, F. Epron, Effect of higher alcohols on the performances of a 1%Rh/$MgAl_2O_4$/Al_2O_3 catalyst for hydrogen production by crude bioethanol steam reforming, Int. J. Hydrogen Energy 36 (2011) 311–318, http://dx.doi.org/10.1016/j.ijhydene.2010.09.039.

[9] E.M. Green, Fermentative production of butanol-the industrial perspective, Curr. Opin. Biotechnol. 22 (2011) 337–343, http://dx.doi.org/10.1016/j.copbio.2011.02.004.

[10] W. Cai, P.R. de la Piscina, N. Homs, Hydrogen production from the steam reforming of bio-butanol over novel supported Co-based bimetallic catalysts, Bioresour. Technol. 107 (2012) 482–486, http://dx.doi.org/10.1016/j.biortech.2011.12.081.

[11] W. Cai, N. Homs, P. Ramirez de la Piscina, Efficient hydrogen production from bio-butanol oxidative steam reforming over bimetallic Co–Ir/ZnO catalysts, Green Chem. 14 (2012) 1035, http://dx.doi.org/10.1039/c2gc16369a.
[12] W. Cai, P.R.D. La Piscina, K. Gabrowska, N. Homs, Hydrogen production from oxidative steam reforming of bio-butanol over coIr-based catalysts: effect of the support, Bioresour. Technol. 128 (2013) 467–471, http://dx.doi.org/10.1016/j.biortech.2012.10.125.
[13] W. Cai, N. Homs, P. Ramirez de la Piscina, Renewable hydrogen production from oxidative steam reforming of bio-butanol over CoIr/$CeZrO_2$ catalysts: relationship between catalytic behaviour and catalyst structure, Appl. Catal. B Environ. 150–151 (2014) 47–56, http://dx.doi.org/10.1016/j.apcatb.2013.11.032.
[14] W. Cai, P.R. de la Piscina, N. Homs, Oxidative steam reforming of bio-butanol for hydrogen production: effects of noble metals on bimetallic CoM/ZnO catalysts (M = Ru, Rh, Ir, Pd), Appl. Catal. B Environ. 145 (2014) 56–62, http://dx.doi.org/10.1016/j.apcatb.2013.03.016.
[15] K. Takanabe, K. Aika, K. Seshan, L. Lefferts, Sustainable hydrogen from bio-oil—Steam reforming of acetic acid as a model oxygenate, J. Catal. 227 (2004) 101–108, http://dx.doi.org/10.1016/j.jcat.2004.07.002.
[16] K. Takanabe, K. Aika, K. Inazu, T. Baba, K. Seshan, L. Lefferts, Steam reforming of acetic acid as a biomass derived oxygenate: bifunctional pathway for hydrogen formation over Pt/ZrO2 catalysts, J. Catal. 243 (2006) 263–269, http://dx.doi.org/10.1016/j.jcat.2006.07.020.
[17] F. Bimbela, M. Oliva, J. Ruiz, L. García, J. Arauzo, Hydrogen production by catalytic steam reforming of acetic acid, a model compound of biomass pyrolysis liquids, J. Anal. Appl. Pyrol. 79 (2007) 112–120, http://dx.doi.org/10.1016/j.jaap.2006.11.006.
[18] B. Matas Güell, I. Babich, K. Seshan, L. Lefferts, Steam reforming of biomass based oxygenates—mechanism of acetic acid activation on supported platinum catalysts, J. Catal. 257 (2008) 229–231, http://dx.doi.org/10.1016/j.jcat.2008.04.019.
[19] B. Matas Güell, I.M.T. Da Silva, K. Seshan, L. Lefferts, Sustainable route to hydrogen—design of stable catalysts for the steam gasification of biomass related oxygenates, Appl. Catal. B Environ. 88 (2009) 59–65, http://dx.doi.org/10.1016/j.apcatb.2008.09.018.
[20] K. Polychronopoulou, C.N. Costa, A.M. Efstathiou, The steam reforming of phenol reaction over supported-Rh catalysts, Appl. Catal. A Gen. 272 (2004) 37–52, http://dx.doi.org/10.1016/j.apcata.2004.05.002.
[21] K. Polychronopoulou, J. Fierro, A. Efstathiou, The phenol steam reforming reaction over MgO-based supported Rh catalysts, J. Catal. 228 (2004) 417–432, http://dx.doi.org/10.1016/j.jcat.2004.09.016.
[22] K. Polychronopoulou, A.M. Efstathiou, Spillover of labile OH, H, and O species in the H2 production by steam reforming of phenol over supported-Rh catalysts, Catal. Today 116 (2006) 341–347, http://dx.doi.org/10.1016/j.cattod.2006.05.079.
[23] K. Polychronopoulou, C.N. Costa, A.M. Efstathiou, The role of oxygen and hydroxyl support species on the mechanism of H2 production in the steam reforming of phenol over metal oxide-supported-Rh and -Fe catalysts, Catal. Today 112 (2006) 89–93, http://dx.doi.org/10.1016/j.cattod.2005.11.037.
[24] K. Polychronopoulou, K. Giannakopoulos, A.M. Efstathiou, Tailoring MgO-based supported Rh catalysts for purification of gas streams from phenol, Appl. Catal. B Environ. 111–112 (2012) 360–375, http://dx.doi.org/10.1016/j.apcatb.2011.10.019.
[25] A. Oasmaa, D. Meier, Norms and standards for fast pyrolysis liquids, J. Anal. Appl. Pyrolysis 73 (2005) 323–334, http://dx.doi.org/10.1016/j.jaap.2005.03.003.
[26] S. Sá, H. Silva, L. Brandão, J.M. Sousa, A. Mendes, Catalysts for methanol steam reforming—a review, Appl. Catal. B Environ. 99 (2010) 43–57, http://dx.doi.org/10.1016/j.apcatb.2010.06.015.
[27] X. Hu, G. Lu, Investigation of the Effects of Molecular Structure on Oxygenated Hydrocarbon Steam Re-forming, (2009) 5851–5858.
[28] F. Bimbela, M. Oliva, J. Ruiz, L. García, J. Arauzo, Catalytic steam reforming of model compounds of biomass pyrolysis liquids in fixed bed: acetol and *n*-butanol, J. Anal. Appl. Pyrolysis 85 (2009) 204–213, http://dx.doi.org/10.1016/j.jaap.2008.11.033.
[29] F. Bimbela, D. Chen, J. Ruiz, L. García, J. Arauzo, Ni/Al coprecipitated catalysts modified with magnesium and copper for the catalytic steam reforming of model compounds from biomass pyrolysis liquids, Appl. Catal. B Environ. 119-120 (2012) 1–12, http://dx.doi.org/10.1016/j.apcatb.2012.02.007.
[30] J.A. Medrano, M. Oliva, J. Ruiz, L. García, J. Arauzo, Catalytic steam reforming of butanol in a fluidized bed and comparison with other oxygenated compounds, Fuel Process. Technol. 124 (2014) 123–133, http://dx.doi.org/10.1016/j.fuproc.2014.02.022.
[31] K. Bizkarra, V.L. Barrio, J.R. Yartu, P.L.A. equies, J.F.C. rias, Hydrogen production from *n*-butanol over alumina and modified alumina nickel catalysts, Int. J. Hydrogen Energy (2015) 1–9, http://dx.doi.org/10.1016/j.ijhydene.2015.01.055.
[32] H. Harju, J. Lehtonen, L. Lefferts, Steam- and autothermal-reforming of n-butanol over Rh/ZrO_2 catalyst, Catal. Today 244 (2015) 47–57, http://dx.doi.org/10.1016/j.cattod.2014.08.013.
[33] S. Hartley, P. Amornraksa, N. Kim-Lohsoontorn, Thermodynamic analysis and experimental study of hydrogen production from oxidative reforming of *n*-butanol, Chem. Eng. J. (2015), http://dx.doi.org/10.1016/j.cej.2015.02.016.
[34] J. Rostrup-Nielsen, Catalytic steam reforming, in: J. Anderson, M. Boudart (Eds.), Catal SE-1, Springer, Berlin, Heidelberg, 1984, pp. 1–117, http://dx.doi.org/10.1007/978-3-642-93247-2_1.
[35] M. Benito, R. Padilla, L.R. Serrano-Lotina, J.J.B. odriguez, L.D. rey, The role of surface reactions on the active and selective catalyst design for bioethanol steam reforming, J. Power Sources 192 (2009) 158–164, http://dx.doi.org/10.1016/j.jpowsour.2009.02.015.
[36] M.B. Valenzuela, C.W. Jones, P.K. Agrawal, Batch aqueous-phase reforming of woody biomass, Energy Fuels 20 (2006) 1744–1752, http://dx.doi.org/10.1021/ef060113p.
[37] R.K. Kaila, A. Gutiérrez, S.T. Korhonen, A.O.I. Krause, Autothermal reforming of n-dodecane, toluene, and their mixture on mono- and bimetallic noble metal zirconia catalysts, Catal. Lett. 115 (2007) 70–78, http://dx.doi.org/10.1007/s10562-007-9075-z.
[38] R.K. Kaila, A. Gutiérrez, R. Slioor, M. Kemell, M. Leskelä, A.O.I. Krause, Zirconia-supported bimetallic RhPt catalysts: characterization and testing in autothermal reforming of simulated gasoline, Appl. Catal. B Environ. 84 (2008) 223–232, http://dx.doi.org/10.1016/j.apcatb.2008.04.001.
[39] E. Guglielminotti, F. Pinna, M. Rigoni, G. Strukul, L. Zanderighi, The effect of iron on the activity and the selectivity of Rh/ZrO_2 catalysts in the CO hydrogenation, J. Mol. Catal. A Chem. 103 (1995) 105–116, http://dx.doi.org/10.1016/1381-1169(95) 119-0.
[40] D.E. Mears, Tests for transport limitations in experimental catalytic reactors, Ind. Eng. Chem. Process Des. Dev. 10 (1971) 541–547, http://dx.doi.org/10.1021/i260040a020.
[41] P.B. Weisz, C.D. Prater, Interpretation of measurements in experimental catalysis, Adv. Catal. 6 (1954) 143–196, http://dx.doi.org/10.1016/S0360-0564(08)60390-9.
[42] T.A. Nijhuis, S.J. Tinnemans, T. Visser, B.M. Weckhuysen, Towards real-time spectroscopic process control for the dehydrogenation of propane over supported chromium oxide catalysts, Chem. Eng. Sci. 59 (2004) 5487–5492, http://dx.doi.org/10.1016/j.ces.2004.07.103.
[43] A. Iglesias-Juez, A.M. Beale, K. Maaijen, T.C. Weng, P. Glatzel, B.M. Weckhuysen, A combined in situ time-resolved UV–Vis, Raman and high-energy resolution X-ray absorption spectroscopy study on the deactivation behavior of Pt and PtSn propane dehydrogenation catalysts under industrial reaction conditions, J. Catal. 276 (2010) 268–279, http://dx.doi.org/10.1016/j.jcat.2010.09.018.
[44] S. Sokolov, M. Stoyanova, U. Rodemerck, D. Linke, E.V. Kondratenko, Effect of support on selectivity and on-stream stability of surface VOx species in non-oxidative propane dehydrogenation, Catal. Sci. Technol. 4 (2014) 1323, http://dx.doi.org/10.1039/c3cy01083j.
[45] V. Macho, M. Králik, E. Jurecekova, J. Hudec, L. Jurecek, Dehydration of C4 alkanols conjugated with a positional and skeletal isomerisation of the formed C4 alkenes, Appl. Catal. A Gen. 214 (2001) 251–257, http://dx.doi.org/10.1016/s0926-860x(01)497-5.
[46] T. Viinikainen, I. Kauppi, S. Korhonen, L. Lefferts, J. Kanervo, J. Lehtonen, Molecular level insights to the interaction of toluene with ZrO2-based biomass gasification gas clean-up catalysts, Appl. Catal. B Environ. 142–143 (2013) 769–779, http://dx.doi.org/10.1016/j.apcatb.2013.06.008.
[47] G. Macnab, The hydroisomerization of n-butenes: I. The reaction of 1-butene over alumina-and silica-supported rhodium catalysts, J. Catal. 10 (1968) 19–26, http://www.sciencedirect.com/science/article/pii/0021951768902182 (accessed 10.02.15).
[48] S. Mostafa, J.R. Croy, H. Heinrich, B.R. Cuenya, Catalytic decomposition of alcohols over size-selected Pt nanoparticles supported on ZrO2: a study of activity, selectivity, and stability, Appl. Catal. A Gen. 366 (2009) 353–362, http://dx.doi.org/10.1016/j.apcata.2009.07.028.
[49] W. Shen, G.A. Tompsett, R. Xing, W. Curtis Conner, G.W. Huber, Vapor phase butanal self-condensation over unsupported and supported alkaline earth metal oxides, J. Catal. 286 (2012) 248–259, http://dx.doi.org/10.1016/j.jcat.2011.11.009.
[50] Y. Bie, A. Gutierrez, T.R. Viljava, J.M. Kanervo, J. Lehtonen, Hydrodeoxygenation of methyl heptanoate over noble metal catalysts: catalyst screening and reaction network, Ind. Eng. Chem. Res. 52 (2013) 11544–11551, http://dx.doi.org/10.1021/ie4012485.
[51] A. Gangadharan, M. Shen, T. Sooknoi, D.E. Resasco, R.G. Mallinson, Condensation reactions of propanal over CexZr1−xO2 mixed oxide catalysts, Appl. Catal. A Gen. 385 (2010) 80–91, http://dx.doi.org/10.1016/j.apcata.2010.06.048.
[52] E.I. Gürbüz, E.L. Kunkes, J.A. Dumesic, Integration of C—C coupling reactions of biomass-derived oxygenates to fuel-grade compounds, Appl. Catal. B Environ. 94 (2010) 134–141, http://dx.doi.org/10.1016/j.apcatb.2009.11.001.
[53] M. Virginie, M. Araque, A.-C. Roger, J.C. Vargas, A. Kiennemann, Comparative study of H2 production by ethanol steam reforming on Ce2Zr1. 5Co0. 5O8-δ and Ce2Zr1. 5Co0. 47Rh0. 07O8-δ: evidence of the Rh role on the deactivation process, Catal. Today 138 (2008) 21–27, http://dx.doi.org/10.1016/j.cattod.2008.04.047.
[54] A. Roine, HSC Chemistry, 2007.